Breathers in a discrete nonlinear Schrödinger-type model: Exact stability results

Avijit Lahiri,[1] Subhendu Panda,[2] and Tarun K. Roy[2]

[1]*Department of Physics, Vidyasagar Evening College, Kolkata 700 006, India*
[2]*Saha Institute of Nuclear Physics, 1/AF, Bidhannagar, Kolkata 700 064, India*

Following our earlier work [Phys. Rev. Lett. **84**, 3570 (2000)] we present an exact linear stability analysis of one-site monochromatic breathers in a piecewise smooth discrete nonlinear Schrödinger-type model. Destabilization of the breather occurs by virtue of a growth rate becoming positive as a stability border is crossed, while above a critical spatial decay rate (λ_c) the breather is found to be intrinsically unstable. The model admits of other exact breather solutions, including multisite monochromatic breathers for which the profile variable (ϕ_n) crosses a relevant threshold at more than one site. In particular, we consider exact two-site breather solutions with phase difference δ between the two sites above threshold, and present stability results for $\delta = \pi$ (antiphase breather; the in-phase breather with $\delta = 0$ happens to be intrinsically unstable). We obtain a band of extended eigenmodes, together with a pair of localized symmetric modes and another pair of localized antisymmetric ones. The frequencies of the localized modes vary as the parameters characterizing the breather are made to vary, and destabilization occurs through the Krein collision of a quartet of growth rates, leading to temporal growth of a pair of symmetric eigenmodes of nonzero frequency. We clarify the limit $N \to \infty$ (N is the gap length between the sites above threshold) when the two-site breather reduces to a pair of decoupled one-site breathers. The model offers the possibility of obtaining spatially random vortex-type breathers.

I. INTRODUCTION

The discrete nonlinear Schrödinger (DNLS) equation, also known as the discrete self-trapping model, has claimed wide attention in the literature, modeling a great variety of situations (see [1–7] for a review and for relevant background). These include excitations in macromolecules [8–10] self-trapping of electrons in a lattice [11], absorption in waveguides [12], and the leading order approximation in the nonlinear discrete Klein-Gordon (NDKG) model [1]. Beginning from the existence proof of MacKay and Aubry [13], a large body of numerical and analytical work has accumulated relating to the existence proof of breathers, their numerical construction, and exploration of their characteristics, especially their dynamical stability. However, exact construction of and exact stability results on breathers in DNLS-type models are rare in the literature. In this context, we considered in [14] a piecewise smooth (PWS) variant of the DNLS equation (as also of the NDKG equation), obtaining exact one-site breather solutions by referring to the stable and unstable manifolds of a hyperbolic fixed point of an associated mapping. The model we consider is of the general DNLS form

$$i\frac{d\psi_n}{dt} + V(\psi_{n+1} + \psi_{n-1}) = \psi_n f(|\psi_n|), \qquad (1)$$

with nearest neighbor coupling parameter $V(>0)$ and with the function $f(x)$ given by

$$f(x) = -\gamma\left(1 - \frac{a}{x}\right)\Theta(x-a) \quad (x>0), \qquad (2)$$

which is to be compared with the more usual form

$$f(x) = -\gamma x^2 \qquad (3)$$

in the cubic DNLS model.

In Eq. (2), Θ stands for the Heaviside step function, γ is a parameter indicating the strength of nonlinearity, and a (>0) plays the role of a threshold parameter which in the following we scale to $a=1$. In the following, for convenience in presenting our figures we treat all parameters and variables as dimensionless. Figure 1 compares the function $f(x)$ of Eq. (2) with that of Eq. (3) to bring out the qualitative similarity in their nature. Assuming that Eq. (1) admits of a monochromatic breather solution of the form

$$\psi_n = \phi_n e^{-i\omega t}, \qquad (4)$$

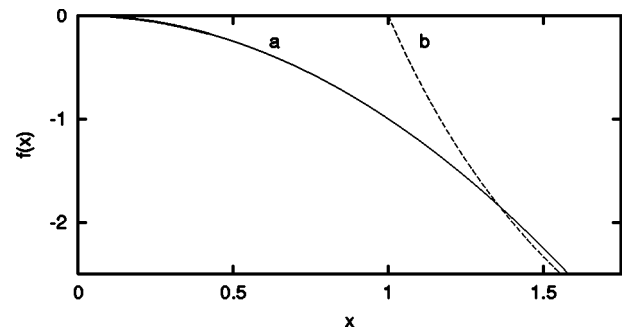with real-valued profile variables ϕ_n, one finds that the ϕ_n's satisfy the mapping

FIG. 1. Comparison of function $f(x)$ (*a*) of the usual form $f(x) = -\gamma|x|^2$ ($\gamma=1$) with (*b*) of Eq. (2), for an appropriately scaled γ.

$$\phi_{n+1} + \omega\phi_n + \phi_{n-1} = -\gamma[\phi_n - \text{sgn}(\phi_n)]\Theta(\phi_n - 1). \tag{5}$$

The stable and unstable manifolds of the mapping emanating from $\phi_n = \phi_{n-1} = 0$ (this corresponds to a hyperbolic point of the mapping for $|\omega| > 2$) consist of linear pieces, and homoclinic points can be obtained exactly, thereby leading to exact breather solutions. The parameter a ($=1$ in our calculations) plays the role of a threshold in the model, and different types of breather solutions correspond to the number and locations of lattice sites at which the profile variable ϕ_n crosses the threshold ($|\phi_n| > a$); such sites will be termed *high*, while sites with $|\phi_n| < a$ will be termed *low*. For instance, a one-site breather with only one high site at $n = 0$ is given by

$$\bar{\psi}_n = \frac{\gamma\lambda^{|n|}}{\gamma + \lambda - 1/\lambda} e^{-i\omega t}, \tag{6}$$

where ω, γ (appropriately scaled in terms of V, see below) and the spatial decay rate λ ($|\lambda| < 1$) satisfy

$$|\omega| > 2, \quad \omega = -(\lambda + 1/\lambda), \tag{7}$$

$$\omega\gamma < 0, \quad |\gamma| > 1 + 1/|\lambda|. \tag{8}$$

[Note: Eqs. (10) and (11) in [14] expressing the above relations contained errors due to oversight, which we regret.] We distinguish between breathers of *type A* ($\lambda > 0, \omega < -2$) and *type B* ($\lambda < 0, \omega > 2$), referring to the former in presenting our results below (results for type B are obtained analogously). The overbar in Eq. (6) is used here to distinguish the breather solutions from neighboring perturbed solutions (see below).

As mentioned in [14], the problem of dynamical stability of the breathers (6) can be solved exactly, and the present paper is devoted to this exact stability analysis for the one-site breathers (Sec. II) as also for two-site antiphase breathers (see below) which we construct in Sec. III. We show that the destabilization of the latter (Sec. IV) involves an interesting Krein collision of eigenvalues, as opposed to destabilization of the one-site breathers through the double-zero eigenvalue. All the eigenmodes and eigenvalues can be obtained exactly in the model, thereby yielding a complete solution to the problem of breather stability. This complements the body of numerical stability results (see, e.g., [15–20]) in the literature, and may serve to identify key features of breather stability in more realistic models. One notes in this context that the stability analysis of discrete breathers was initiated in a major way by Aubry [21] (see also [22]), who introduced a number of insights, including an interesting interpretation of the key concept of the Krein signature. An overview of early work on breather stability is to be found in [1].

II. STABILITY OF ONE-SITE BREATHERS

We consider perturbations in the "rotating frame" to the breather solution of the form

$$\psi_n = \bar{\psi}_n + u_n(t)e^{-i\omega t}. \tag{9}$$

Splitting u_n into real and imaginary parts

$$u_n = x_n + iy_n, \tag{10}$$

substituting in Eqs. (1) and (2) and linearizing, we obtain

$$-\frac{1}{V}\dot{y}_n + (x_{n+1} + x_{n-1}) + \omega x_n + \gamma x_0 \delta_{n,0} = 0, \tag{11}$$

$$\frac{1}{V}\dot{x}_n + (y_{n+1} + y_{n-1}) + \omega y_n + \gamma y_0\left(1 - \frac{1}{b}\right)\delta_{n,0} = 0, \tag{12}$$

where $b = \gamma/(\gamma + \lambda - 1/\lambda)$, and where γ and ω ($= -\lambda - 1/\lambda$) have been scaled in terms of V to $\omega/V \to \omega$, $\gamma/V \to \gamma$, which is equivalent to scaling the eigenvalues μ (see below) by V^2. With these rescalings, Eqs. (11) and (12) result from the Hamiltonian

$$H = \sum_n \left\{ (x_{n+1}x_n + y_{n+1}y_n) + \frac{\omega}{2}(x_n^2 + y_n^2) \right\}$$
$$+ \frac{\gamma}{2}\left\{ x_0^2 + y_0^2\left(1 - \frac{1}{b}\right) \right\}. \tag{13}$$

The growth rates of perturbations as also the associated eigenvectors can all be calculated from Eqs. (11) and (12).

One can eliminate the y_n's (x_n's) to obtain a second order system in x_n's (y_n's) in the form

$$\ddot{X} = AX, \quad \ddot{Y} = A^T Y, \tag{14}$$

where the x_n's and y_n's have been combined into single bi-infinite columns $X = (\ldots, x_{-2}, x_{-1}, x_0, x_1, x_2, \ldots)^T$, $Y = (\ldots, y_{-2}, y_{-1}, y_0, y_1, y_2, \ldots)^T$, and A is a banded matrix with elements a_{mn} ($-\infty < m, n < \infty$) differing from 0 only when $|m - n| \leq 2$:

$$a_{0,0} = 2(\gamma\lambda - 2 - \lambda^2), \tag{15a}$$

$$a_{0,1} = a_{0,-1} = 3\lambda + 1/\lambda, \tag{15b}$$

$$a_{1,0} = a_{-1,0} = 2\lambda + 2/\lambda - \gamma, \tag{15c}$$

$$a_{n,n} = -(\lambda^2 + 1/\lambda^2 + 4), \quad (n \neq 0), \tag{15d}$$

$$a_{n,n+1} = a_{n+1,n} = 2(\lambda + 1/\lambda), \quad (n \neq 0,1), \tag{15e}$$

$$a_{n,n+2} = a_{n+2,n} = -1. \tag{15f}$$

The eigenvalues (μ) of A are related to growth rates (p) of perturbations [refer to Eqs. (11) and (12)] through

$$\mu = p^2, \tag{16}$$

and can be real negative, real positive, or complex, the last occurring with complex conjugate partners. Correspondingly, the spectrum of growth rates (these, in turn, are related in a simple manner to the Floquet multipliers considered in [21]) can include of a purely imaginary pair ($p = \pm i\sqrt{-\mu}$), a real pair ($\pm\sqrt{\mu}$), or a quartet of the form ($\pm v \pm iw, v$ and w real), respectively. If the spectrum of growth rates is made up

entirely of pairs of the first type (i.e., the eigenvalues μ are all real and negative) the breather (4) will be linearly stable. In the following we shall refer to eigenvalues of A while the corresponding eigenmodes of perturbations can be obtained from Eqs. (11) and (12); the real parts of the latter are the eigenvectors of A (the imaginary parts being the corresponding eigenvectors of A^T), which we consider below. A real and negative eigenvalue of A may be associated with either a *localized* or an *extended* eigenmode. The eigenvalues corresponding to extended modes form a band. A typical mode belonging to a band is of the form

$$x_n = \begin{cases} a_1 \cos n\theta + a_2 \sin n\theta + a_3 \chi^n & (n \geq 0), \quad (17\text{a}) \\ b_1 \cos n\theta + b_2 \sin n\theta + b_3 \chi^{-n} & (n \leq 0). \quad (17\text{b}) \end{cases}$$

Here θ $(0 \leq \theta \leq \pi)$ is determined by

$$(2 \cos \theta + \omega)^2 + \mu = 0, \tag{18}$$

corresponding to a running wave far away from the breather, and the band of eigenvalues μ extends from $-(\omega-2)^2$ to $-(\omega+2)^2$ (recall that all our results are for type A breathers). For any μ within this band, the relation

$$(\chi + 1/\chi + \omega)^2 + \mu = 0 \tag{19}$$

gives one single real solution for χ satisfying $|\chi| < 1$, and it is this value that occurs in Eqs. (17a) and (17b), giving the deviation of the eigenmode from a running wave close to the location of the breather (i.e., the site $n=0$). While Eqs. (17a) and (17b) identically satisfy the eigenvalue equation

$$\sum a_{nm} x_m = \mu x_n \tag{20}$$

for $|n| \geq 2$, the constants $a_i, b_i (i=1,2,3)$ are to be determined from Eq. (20) with $|n| \leq 1$ and from the matching condition

$$a_1 + a_3 = b_1 + b_3. \tag{21}$$

One finds that each eigenvalue μ in the interior of the band $(0 < \theta < \pi)$ is doubly degenerate while, for a given λ, the band edges are empty except when γ satisfies (for the inner band edge $\theta = 0$)

$$\gamma = \gamma_1(\lambda) = \frac{(\lambda - 1/\lambda)\sqrt{[(\lambda + 1/\lambda)^2 - 2(\lambda + 1/\lambda)]}}{(\lambda - 1/\lambda) + \sqrt{[(\lambda + 1/\lambda)^2 - 2(\lambda + 1/\lambda)]}}, \tag{22}$$

or (for the outer band edge $\theta = \pi$)

$$\gamma = \gamma_2(\lambda) = \frac{(\lambda - 1/\lambda)\sqrt{[(\lambda + 1/\lambda)^2 + 2(\lambda + 1/\lambda)]}}{(\lambda - 1/\lambda) + \sqrt{[(\lambda + 1/\lambda)^2 + 2(\lambda + 1/\lambda)]}}, \tag{23}$$

in which case the band is occupied by a single mode. For real negative μ lying outside the band, on the other hand, a typical mode is of the form

$$x_n = \begin{cases} a_1 \chi_1^n + a_2 \chi_2^n & (n \geq 0), \quad (24\text{a}) \\ b_1 \chi_1^{-n} + b_2 \chi_2^{-n} & (n \leq 0), \quad (24\text{b}) \end{cases}$$

and is localized, $\chi_{1,2}$ being those two roots of Eq. (19) that satisfiy $|\chi| < 1$. Once again, the constants $a_i, b_i (i=1,2)$ are to be determined on substituting in Eq. (20). One finds that possible solutions correspond to spatially *symmetric* as well as *antisymmetric* eigenmodes. For a symmetric mode one has $a_1 = b_1, a_2 = b_2$ and μ is related to γ, λ through the relation

$$\gamma = \frac{A_2 B_1 - A_1 B_2}{(A_1 - A_2) + 2\lambda(B_1 - B_2)}, \tag{25}$$

where

$$A_{1,2} = 2\chi_{1,2}^2 - 2\left(3\lambda + \frac{1}{\lambda}\right)\chi_{1,2} + 2\lambda^2 + 4 + \mu, \tag{26a}$$

$$B_{1,2} = \chi_{1,2}^3 - 2\left(\lambda + \frac{1}{\lambda}\right)\chi_{1,2}^2 + \left(\lambda^2 + \frac{1}{\lambda^2} + 5 + \mu\right)\chi_{1,2}$$
$$- 2\left(\lambda + \frac{1}{\lambda}\right). \tag{26b}$$

The existence of an antisymmetric mode, on the other hand, requires

$$\mu + (\chi_1 + \chi_2 + \omega)^2 + 1 - \chi_1 \chi_2 = 0. \tag{27}$$

One has to note in this connection that the existence of a type A breather additionally requires [see Eq. (8)]

$$\gamma > \gamma_0(\lambda) = 1 + 1/\lambda. \tag{28}$$

For any given λ and γ $[> \gamma_0(\lambda)]$ lying within a certain range (see below), Eq. (25) implies the existence of a *single* symmetric localized mode with the eigenvalue μ lying in the range

$$-(\omega+2)^2 < \mu < 0. \tag{29}$$

One finds that, as μ approaches the inner band edge $-(\omega +2)^2$, γ approaches $\gamma_1(\lambda)$ of Eq. (22).

On the other hand, μ approaches the *stability limit* ($\mu = 0$) as γ approaches

$$\bar{\gamma}(\lambda) = \frac{(1 + 4\lambda^2 + \lambda^4)(1 - \lambda^2)}{2\lambda^3}. \tag{30}$$

This result is obtained from Eq. (25) by expanding $A_{1,2}$ and $B_{1,2}$ [of Eqs. (26a) and (26b)] as power series in μ for small $|\mu|$, and retaining terms up to degree three, since higher degree terms are found to be irrelevant in the limit $|\mu| \to 0$.

Thus, for γ lying in the range

$$\gamma_1(\lambda) < \gamma < \bar{\gamma}(\lambda), \tag{31}$$

there exists a single localized mode in addition to a band of extended modes and, subject to the existence condition (28), the breather is stable. The localized mode is spatially sym-
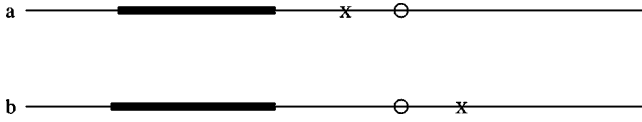
FIG. 2. Spectrum of eigenvalues of matrix A for (a) $\gamma_1(\lambda) < \gamma < \bar{\gamma}(\lambda)$ and (b) $\gamma > \bar{\gamma}(\lambda)$; the cross denotes eigenvalue for the isolated localized mode while the thick black line denotes the band; the circle corresponds to $\mu = 0$.

FIG. 3. Disposition of growth rates p in the complex plane with (a) $\gamma < \bar{\gamma}$ and (b) $\gamma > \bar{\gamma}$.

metric, and the possibility of an antisymmetric mode appearing in the model is ruled out on the grounds that Eq. (27) does not actually possess a real negative solution for μ. Noting similarly that Eq. (23) is inconsistent with Eq. (28) for all λ in the range $0 < \lambda < 1$, one arrives at Fig. 2(a) depicting the spectrum of eigenvalues when γ satisfies Eq. (31). The value $\gamma = \gamma_1(\lambda)$ is the threshold for the localized mode while $\gamma = \bar{\gamma}(\lambda)$ corresponds to destabilization of the breather. The only mode of destabilization of the breather (6) is through the double-zero eigenvalue $\mu = 0$. In this context one notes that the eigenvalue $\mu = 0$ exists for all parameter values in the model, the corresponding eigenmode being

$$x_n = 0, \quad y_n = |\bar{\psi}_n|. \tag{32}$$

At $\gamma = \bar{\gamma}(\lambda)$ this corresponds to a doubly degenerate eigenvalue. However, this eigenmode is quite distinct from the eigenvector of A that also happens to exist for all λ, γ. Indeed, Eqs. (11) and (12) no longer imply Eq. (20) for $\mu = 0$. Still, A possesses an eigenvector of the form

$$x_n = \lambda^{|n|}(\alpha + |n|\beta), \tag{33}$$

as can be checked directly from Eqs. (15a)–(15f), the ratio of α to β being given by

$$\frac{\alpha}{\beta} = \frac{1 + \lambda^2}{1 - \lambda^2 - \gamma\lambda}. \tag{34}$$

As mentioned, this represents a spurious eigenmode in the context of Eqs. (11) and (12). As γ crosses the stability border $\bar{\gamma}(\lambda)$, the eigenvalue μ corresponding to the localized mode becomes positive, thereby giving rise to a positive growth rate and implying destabilization of the breather [the trivial eigenvalue $\mu = 0$ with eigenmode (32) continues to exist]. The corresponding localized eigenmode is now of the form

$$x_n = \begin{cases} a\chi^n + a^*\chi^{*n} & (n \geq 0), & (35a) \\ b\chi^{-n} + b^*\chi^{*-n} & (n \leq 0), & (35b) \end{cases}$$

where χ and χ^* represent the complex conjugate pair of solutions of Eq. (19) (recall that $\mu > 0$), with $|\chi| < 1$. The coefficients a, b can once again be obtained exactly from Eq. (20), thereby yielding the growing mode beyond the instability. Once again, this mode happens to be symmetric ($a = b$).
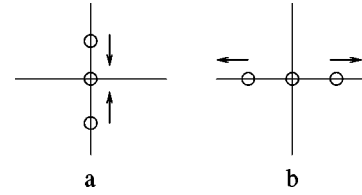
Figure 2 depicts the disposition of eigenvalues μ on either side of destabilization, while Fig. 3 indicates how the disposition of growth rates [p of Eq. (16)] in the complex plane changes across the destabilization border.

Figure 4 depicts the λ-γ parameter space for the model together with the curves C_1 [$\gamma = \gamma_0(\lambda) \equiv 1 + 1/\lambda$], C_2 [$\gamma = \bar{\gamma}(\lambda)$], and C_3 [$\gamma = \gamma_1(\lambda)$]. The breather exists only for points lying above C_1 and is stable only for points lying below C_2, i.e., for (λ, γ) lying between C_1 and C_2 the model admits of a stable breather solution. The curve C_3 gives the *threshold* for the localized mode. Interestingly, the model predicts the existence of a critical value (λ_c) of the spatial decay rate corresponding to the intersection of C_1 and C_2 ($\lambda_c \approx 0.6948$) so that the breathers with $\lambda > \lambda_c$ are unstable for *all* values of the strength of nonlinearity γ [$> \gamma_0(\lambda)$].

We show in Fig. 5(a) the temporal evolution according to Eqs. (1) and (2) of a profile initially ($t = 0$) coinciding with Eq. (6), with (λ, γ) in the region between C_1 and C_2, while Fig. 5(b) shows similar evolution for a breather with $\lambda > \lambda_c$, above C_1. One notes that the breather in Fig. 5(a) performs stable oscillations while that in Fig. 5(b) breaks up within a short time, confirming our results. In this context see also Figs. 4 and 5 of [14].

Finally, one has to reckon with the possibility of complex eigenvalues μ. Note that such complex solutions must occur in complex conjugate pairs (μ, μ^*) and that correspondingly the growth rates p form a quartet of the form indicated ear-
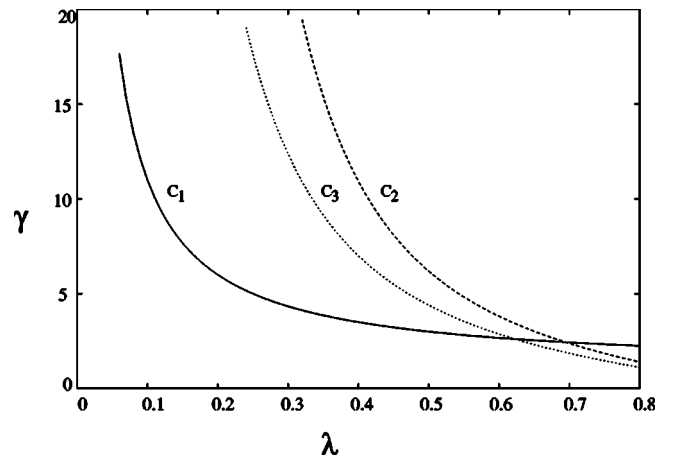

FIG. 4. Curves C_1 [$\gamma = \gamma_0(\lambda)$], C_2 [$\gamma = \bar{\gamma}(\lambda)$], and C_3 [$\gamma = \gamma_1(\lambda)$] in the λ-γ plane; the point of intersection of C_1 and C_2 corresponds to $\lambda = \lambda_c \approx 0.6948$.
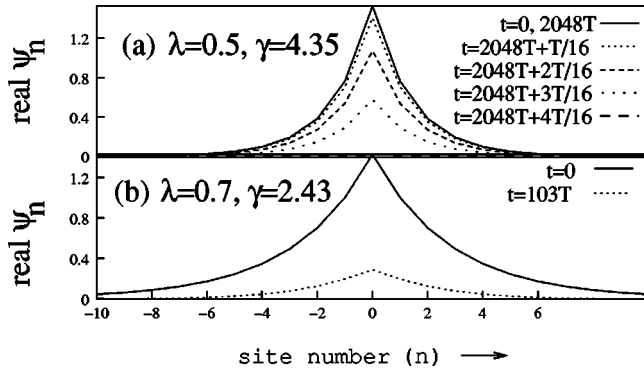
FIG. 5. Numerical integration following Eqs. (1) and (2) of an initial profile given by Eqs. (4) and (6) at $t=0$: (a) $\lambda=0.5$, $\gamma=4.35$ between C_1 and C_3 of Fig. 3—profiles at values of t spanning a quarter of a period ($T/4$) starting from $2048T$; (b) $\lambda=0.7$, just beyond the intersection of C_1 and C_2 in Fig. 3, and $\gamma=2.43$ $[>\gamma_0(\lambda)]$.

lier. For any such μ the corresponding eigenmode has to be a localized one, being of the form (24a) and (24b) where now χ_1,χ_2 are to be complex (such a complex eigenmode is always associated with a complex conjugate mode). A localized mode of this type could again in principle be either symmetric or antisymmetric. It is known that such complex growth rates can arise in Hamiltonian systems through the Hamiltonian Hopf bifurcation (see, e.g., [23]) when eigenvalues of the linearized system (growth rates p in the present context) having opposite Krein signatures [24] collide on the imaginary axis and then move off onto the complex plane (a collision on the real axis is also possible but need not be considered here). Aubry [21] introduced an interesting concept for studying such collisions. Such collisions are, however, ruled out for the one-site breathers for which destabilization occurs not through a complex growth rate but through a real positive one. On the other hand, as we shall see in Sec. V, it is the Krein collision that provides the mode of destabilization of two-site breathers, i.e., localized excitations with two high sites separated by a number of low ones (see next section).

III. TWO-SITE BREATHER SOLUTIONS

As we mentioned in [14], the PWS model (1),(2) is a veritable little laboratory yielding exact breather solutions of a wide variety. For instance, one can construct *two-site* breathers with various possible lengths of the intervening gap N. One other feature of crucial relevance is the relative *phase* between the two sites. This relates to the fact that Eq. (4) admits of an arbitrary phase factor $e^{i\delta}$ that becomes relevant in two-site or multisite breather solutions. Thus, considering a breather with two high sites at $n=0$ and $n=N$ ($|\psi_n|>1$) and all the other sites low ($|\psi_n|<1$), with the high sites having a phase difference of δ, one obtains a monochromatic breather solution of the form (4) with the breather profile ϕ_n now given by

$$\bar{\phi}_n = \begin{cases} b\lambda^{-n} & (n\leq 0), & \text{(36a)} \\ \dfrac{b(1-e^{i\delta}\lambda^N)}{1-\lambda^{2N}}\lambda^n + \dfrac{b(e^{i\delta}-\lambda^N)}{1-\lambda^{2N}}\lambda^{N-n} & & \text{(36b)} \\ & (0\leq n\leq N), \\ be^{i\delta}\lambda^{n-N} & (n\geq N), & \text{(36c)} \end{cases}$$

where

$$b = \frac{\gamma(1-\lambda^{2N})}{\gamma(1-\lambda^{2N})-(1/\lambda-\lambda)(1-\lambda^N e^{i\delta})}. \quad \text{(37)}$$

Here the parameters λ,γ,δ must satisfy a consistency condition (which we do not write down) corresponding to

$$|\phi_0|=|\phi_N|>1, \quad \text{(38a)}$$

$$|\phi_1|=|\phi_{N-1}|<1. \quad \text{(38b)}$$

In particular, a two-site breather located at $n=0,N$ with phase difference $\delta=\pi$ between the high sites is given by

$$\bar{\phi}_n = \begin{cases} \dfrac{b}{1-\lambda^N}(\lambda^n-\lambda^{N-n}) & (0\leq n\leq N), & \text{(39a)} \\ b\lambda^{-n} & (n<0), & \text{(39b)} \\ -b\lambda^{n-N} & (n>N), & \text{(39c)} \end{cases}$$

where

$$b = \frac{\gamma(1-\lambda^N)}{\gamma(1-\lambda^N)-(\lambda^{-1}-\lambda)}, \quad \text{(40)}$$

and λ,γ are to satisfy

$$\gamma > \frac{1+\lambda^{-1}}{1-\lambda^N}. \quad \text{(41)}$$

In the next section we present results on the stability of these two-site antiphase breathers, indicating that the mode of destabilization of these breathers differs essentially from that of the one-site breathers discussed in the last section. The antiphase breathers are also distinct from two-site in-phase breathers ($\delta=0$) in that the latter are always unstable, i.e., the model (1),(2) does not admit of a stable two-site in-phase breather solution.

It is also easy to construct other multisite breather solutions with a larger number of high sites and various lengths of intervening gaps and phase differences between the high sites. The stability analysis of these breathers, however, gets progressively involved with increasing number of sites. It would be interesting to see, for instance, if there exist stable excitations in the model having a *random* spatial structure.

IV. TWO-SITE ANTIPHASE BREATHERS: STABILITY RESULTS

Adopting an approach similar to the stability analysis of one-site breathers we consider perturbations in the rotating frame over the two-site antiphase breather obtained in the last section. The resultant breather variables are

$$\psi_n = [\phi_n + u_n(t)]e^{-i\omega t}, \tag{42}$$

where ϕ_n is given by Eqs. (39a), (39b), and (39c). The variation of the real and imaginary parts of the u_n's is then described by the Hamiltonian

$$H = \sum_n \left\{ (x_{n+1}x_n + y_{n+1}y_n) + \frac{\omega}{2}(x_n^2 + y_n^2) \right\} + \frac{\gamma}{2} \left\{ x_0^2 + x_N^2 \right.$$
$$\left. + (y_0^2 + y_N^2)\left(1 - \frac{1}{b}\right) \right\}. \tag{43}$$

Eliminating the y_n's we again arrive at a matrix equation of the form

$$\ddot{X} = AX, \tag{44}$$

where A is a banded matrix with elements $a_{m,n} = 0$ whenever $|m-n| > 2$, but it includes two 3×3 blocks centered at the $(0,0)$ and (N,N) elements, respectively:

$$a_{0,0} = -\left[2 + \omega^2 + \omega\gamma + (\omega\gamma + \gamma^2)\left(1 - \frac{1}{b}\right)\right], \quad (45a)$$

$$a_{N,N} = -\left[2 + \omega^2 + \omega\gamma + (\omega\gamma + \gamma^2)\left(1 - \frac{1}{b}\right)\right], \quad (45b)$$

$$a_{n,n} = -(2 + \omega^2) \quad (n \neq 0, N), \tag{45c}$$

$$a_{0,1} = a_{N,N+1} = -\left[2\omega + \gamma\left(1 - \frac{1}{b}\right)\right], \tag{45d}$$

$$a_{0,-1} = a_{N,N-1} = -\left[2\omega + \gamma\left(1 - \frac{1}{b}\right)\right], \tag{45e}$$

$$a_{1,0} = a_{N+1,N} = a_{-1,0} = a_{N-1,N} = -(2\omega + \gamma), \quad (45f)$$

$$a_{n,n+1} = a_{n+1,n} = -2\omega \quad (n \neq 0, N), \tag{45g}$$

$$a_{n,n-1} = a_{n-1,n} = -2\omega \quad (n \neq 0, N), \tag{45h}$$

$$a_{n,n+2} = a_{n+2,n} = -1 \quad (n \neq 0, N). \tag{45i}$$

One can now look at the existence of extended and localized eigenmodes as before. In the asymptotic region ($n \to \pm\infty$) an extended mode looks like a running wave $e^{\pm in\theta}e^{\pm\sqrt{\mu}t}$, where μ, an eigenvalue of A, is real and negative. Substituting in Eq. (44) and making use of Eqs. (45a)–(45i) one finds that μ once again satisfies Eq. (18) i.e., the possible eigenvalues μ form a band from $-(\omega-2)^2 < \mu < -(\omega+2)^2$ corresponding to $0 < \theta < \pi$. For any given μ in this range, Eq. (19) also possesses one single real solution

(for the spatial decay rate χ) with $|\chi| < 1$ and thus the extended modes are again of the form (17a),(17b).

Once again the extended modes belong to two classes, namely, symmetric and antisymmetric ones, but now the terms symmetric and antisymmetric refer to $n = 0$ and $n = N$, i.e.,

$$u_n = \begin{cases} u_{N-n} & \text{(symmetric)}, & (46a) \\ -u_{N-n} & \text{(antisymmetric)}. & (46b) \end{cases}$$

While the band of extended modes remains fixed for all γ [subject to Eq. (41)], the eigenvalues of localized modes keep moving along the μ axis as γ is made to vary for any given λ. A typical localized mode is of the form

$$x_n = a_1\chi_1^{-n} + b_1\chi_2^{-n}, \quad (n \leq 0), \tag{47a}$$

$$= a_2\chi_1^{n-N} + b_2\chi_2^{n-N}, \quad (n \geq N), \tag{47b}$$

$$= a_3\chi_1^n + b_3\chi_2^n + a_4\chi_1^{N-n} + b_4\chi_2^{N-n}$$
$$(0 \leq n \leq N), \tag{47c}$$

where a_i, b_i are appropriate constants and $|\chi_1|, |\chi_2| < 1$. Recall that the eigenvalue μ for a localized mode must be outside the band $-(\omega-2)^2 < \mu < -(\omega+2)^2$; additionally, we consider for the present only real negative μ corresponding to which a mode, if it exists, remains bounded with time. As above, a localized mode may be either symmetric or antisymmetric [in the sense of Eqs. (46a) and 46b), respectively]. Using the superscripts s, a to denote symmetric and antisymmetric modes, respectively, one has

$$x_n^{(s,a)} = \begin{cases} a^{(s,a)}\chi_1^{-n} + b^{(s,a)}\chi_2^{-n} & (n \leq 0), & (48a) \\ \pm a^{(s,a)}\chi_1^{n-N} \pm b^{(s,a)}\chi_2^{n-N} & (n \geq N) & (48b) \\ c^{(s,a)}\chi_1^n + d^{(s,a)}\chi_2^n \pm c^{(s,a)}\chi_1^{N-n} \\ \pm d^{(s,a)}\chi_2^{N-n} & (0 \leq n \leq N), & (48c) \end{cases}$$

where the four coefficients $a^{(s,a)}, b^{(s,a)}, c^{(s,a)}, d^{(s,a)}$ satisfy the continuity requirements

$$a^{(s,a)} + b^{(s,a)} = c^{(s,a)}(1 \pm \chi_1^N) + d^{(s,a)}(1 \pm \chi_2^N), \quad (49)$$

and additionally three other equations of the form (20) with $n = \pm 1, 0$. A little algebra then shows that a nontrivial localized mode exists if (λ, γ) satisfy a determinantal condition of the form

$$\det B^{(s,a)} = 0, \tag{50}$$

where $B^{(s,a)}$ is a 4×4 matrix with elements

$$B_{1,1}^{(s,a)} = B_{1,2}^{(s,a)} = 1, \tag{51a}$$

$$B_{1,3}^{(s,a)} = -(1 \pm \chi_1^N), \tag{51b}$$

$$B_{1,4}^{(s,a)} = -(1 \pm \chi_2^N), \tag{51c}$$

$$B_{2,1}^{(s,a)} = \chi_1^2 + (2\omega + k)\chi_1 + 2 + \omega^2 + \omega k + \mu, \quad (51d)$$
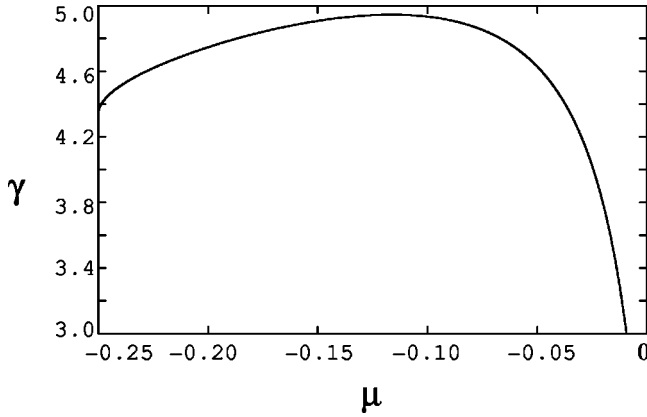
FIG. 6. γ-μ plot as obtained from Eq. (50) for symmetric eigenmodes; $\lambda = 0.5$, $N = 8$.

$$B_{2,2}^{(s,a)} = \chi_2^2 + (2\omega + k)\chi_2 + 2 + \omega^2 + \omega k + \mu, \quad (51e)$$

$$B_{2,3}^{(s,a)} = \chi_1^2 + (2\omega + k)\chi_1 \pm \chi_1^{N-1}(\chi_1^{-1} + 2\omega + k), \quad (51f)$$

$$B_{2,4}^{(s,a)} = \chi_2^2 + (2\omega + k)\chi_2 \pm \chi_2^{N-1}(\chi_2^{-1} + 2\omega + k), \quad (51g)$$

$$B_{3,1}^{(s,a)} = \chi_1 + 2\omega, \quad (51h)$$

$$B_{3,2}^{(s,a)} = \chi_2 + 2\omega, \quad (51i)$$

$$B_{3,3}^{(s,a)} = \chi_1^3 + 2\omega\chi_1^2 + (2 + \omega^2 + \mu)\chi_1 \pm \chi_1^{N-1}(\chi_1^{-2} + 2\omega\chi_1^{-1}$$
$$+ 2 + \omega^2 + \mu), \quad (51j)$$

$$B_{3,4}^{(s,a)} = \chi_2^3 + 2\omega\chi_2^2 + (2 + \omega^2 + \mu)\chi_2 \pm \chi_2^{N-1}(\chi_2^{-2} + 2\omega\chi_2^{-1}$$
$$+ 2 + \omega^2 + \mu), \quad (51k)$$

$$B_{4,1}^{(s,a)} = \chi_1^3 + 2\omega\chi_1^2 + (2 + \omega^2 + \mu)\chi_1 + 2\omega, \quad (51l)$$

$$B_{42}^{(s,a)} = \chi_2^3 + 2\omega\chi_2^2 + (2 + \omega^2 + \mu)\chi_2 + 2\omega, \quad (51m)$$

$$B_{4,3}^{(s,a)} = \chi_1 \pm \chi_1^{N-1}, \quad (51n)$$

$$B_{4,4}^{(s,a)} = \chi_2 \pm \chi_2^{N-1}, \quad (51o)$$

and where $k = \gamma(1 - 1/b)$.

Evaluating this determinant gives us γ as a function of μ for real negative values of μ and one obtains a temporally bounded mode whenever the value of γ satisfies the condition (41). A similar exercise gives us γ as a function of μ for real positive μ as well, and one thus ends up with the following results relating to the breather stability.

(i) A trivial antisymmetric mode exists with $\mu = 0$ for all λ, γ.

(ii) A symmetric mode appears at the inner band edge at a certain threshold value of γ for any given λ; for instance, with $\lambda = 0.5$, $N = 8$, this threshold value occurs at $\gamma_{th}^s \approx 4.333$; with increasing N this threshold increases, until for $N \to \infty$ it approaches the value $\gamma_1(\lambda)$ of Eq. (22) corresponding to the threshold for the one-site breather.
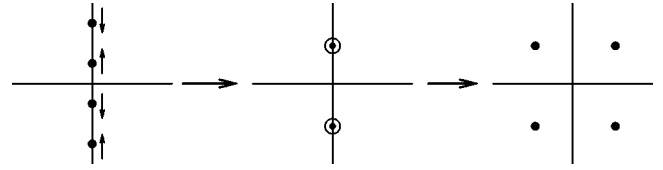

FIG. 7. Disposition of growth rates (p) before and after the Krein collision.

(iii) At the same time, there occurs a symmetric mode with eigenvalue μ closer to $\mu = 0$; with increasing γ it moves in an opposite direction compared to the first symmetric mode, and at a certain value of γ (for given λ) there occurs a *collision* of the two. Figure 6 gives the variation of γ with μ (for fixed λ, N) as obtained from Eqs. (50) and (51) for the symmetric modes, where one finds that, for any given γ, there occur two values of μ (corresponding to the two symmetric modes indicated above) and that the two values coincide at a certain maximum value of γ. In terms of the growth rates (p) this corresponds to a Krein collision [21] leading to instability of the breather. As already mentioned, this instability is associated with what is known as the Hamiltonian Hopf bifurcation in the literature. When considered in terms of Floquet multipliers, this corresponds to the Hamiltonian Hopf bifurcation in mappings, on which there exists a large literature (see, e.g., [24,25]). Denoting the value of γ at the collision as $\gamma_K^s(\lambda, N)$, the question comes up as to what happens for $\gamma > \gamma_K^s$. Here one encounters the possibility of complex eigenvalues (μ) for the system (44),(45a)–(45i). For a complex eigenvalue μ the eigenmode is of the form (47a)–(47c) where χ_1 and χ_2 are again solutions to Eq. (19) satisfying $|\chi_1| = |\chi_2| < 1$, but are now complex; it is associated with a second complex conjugate eigenmode with eigenvalue μ^*. In terms of growth rates (p) this corresponds to a quartet in the complex plane appearing beyond the collision as shown in Fig. 7, and leading to tempo-
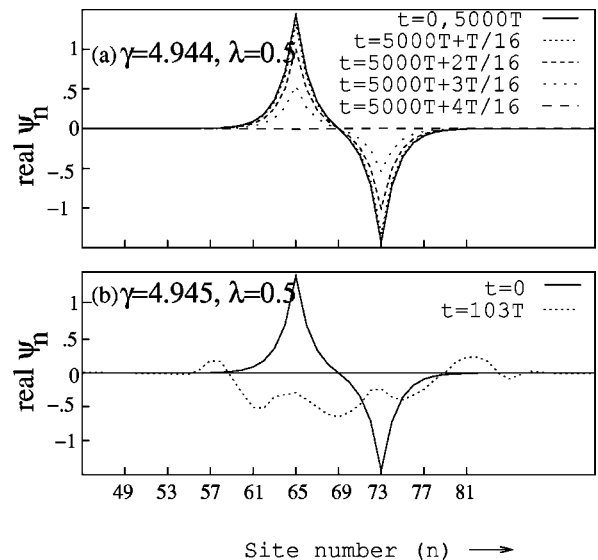

FIG. 8. Numerical integration following Eqs. (1) and (2) of an initial two-site breather profile (with $N = 8$) given by Eqs. (39a)–(39c): (a) $\gamma < \gamma_K^s(\lambda)$ and (b) $\gamma > \gamma_K^s(\lambda)$.
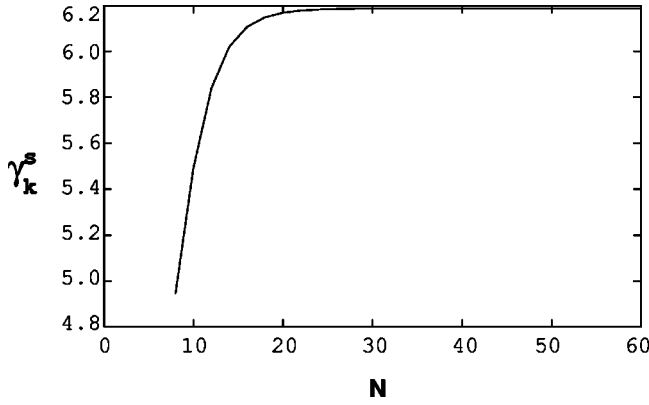
FIG. 9. Variation of the value of γ_K^s with N for a fixed λ ($=0.5$) for the symmetric eigenmodes.

ral growth of the corresponding eigenmode(s). The latter can once again be obtained exactly on substituting the form (48a)–(48c) in Eqs. (44) and (45) and the μ-γ relation is again obtained as a determinant condition similar to Eqs. (50)–(51o) For instance, with $\lambda=0.5$, $N=8$, one has $\gamma_K^s \approx 4.9443$; and for $\gamma=4.9444$ beyond the collision one obtains $\mu=-0.1164\pm0.0012i$.

Figures 8(a) and 8(b) show the evolution according to Eqs. (1) and (2) of a profile corresponding to an exact solution of the form (39a)–(39c) for $\lambda=0.5$, $N=8$; in (a), for which $\gamma=4.944<\gamma_K^s$, the breather is found to oscillate for an indefinitely long period while in (b) the breather is seen to break up quickly for $\gamma=4.945>\gamma_K^s$, in entire conformity with our results.

(iv) For given λ, the bifurcation value γ_K^s increases with N and the value of μ at which the collision occurs gets progressively shifted toward $\mu=0$, until at $N\rightarrow\infty$ γ_K^s approaches the value (30) encountered in the context of the one-site breather (Fig. 9).

(v) For given λ,N, an antisymmetric mode appears across the inner band edge at a certain $\gamma=\gamma_{th}^{(a)}>\gamma_{th}^{(s)}$ (Fig. 10). The eigenvalue for this mode moves toward the trivial eigenvalue $\mu=0$ as γ is made to increase, until at a certain value $\bar{\gamma}(\lambda,N)$ there occurs a double-zero eigenvalue at $\mu=0$. For
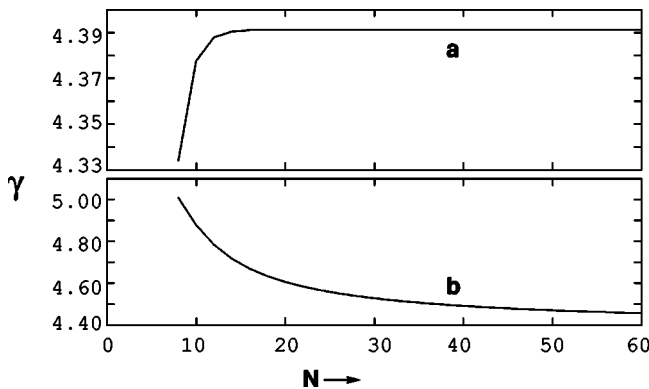

FIG. 10. (a) Variation of γ_{th}^s with N for the symmetric eigenmodes; (b) the corresponding graph for antisymmetric eigenmodes; for either graph $\lambda=0.5$.
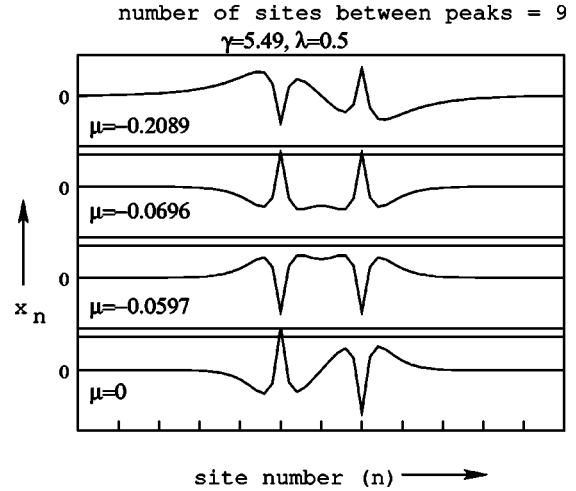

FIG. 11. Symmetric and antisymmetric localized eigenmodes for a two-site breather.

$\gamma>\bar{\gamma}(\lambda,N)$ there results a positive eigenvalue and the mode grows with time. However, one has $\gamma_K^s(\lambda,N)<\bar{\gamma}(\lambda,N)$ and the two-site antiphase breather is destabilized through the Hamiltonian Hopf bifurcation rather than through the double-zero eigenvalue. Figure 11 shows the symmetric and antisymmetric modes as obtained in the above analysis for $\lambda=0.5$, $\gamma=5.490$, and $N=10$.

(vi) As γ is made to increase beyond $\bar{\gamma}(\lambda,N)$, a stage is reached when one has *six* values of the growth rate (p) on the real axis (in addition to the trivial value $p=0$ and the bands on the imaginary axis). The sequential change in the disposition of growth rates in the complex plane typically looks as in Fig. 12.

One notes the interesting manner in which the quartet of complex growth rates collide on the real axis—a phenomenon that can be termed "Krein collision in reverse." In the present context, however, this collision is without significance since the breather has already undergone destabilization before this collision takes place.

(vii) As N is made to increase for a given λ, the value of $\bar{\gamma}(\lambda,N)$ decreases (Fig. 13), until at $N\rightarrow\infty$ it approaches the value $\bar{\gamma}(\lambda)$ of Eq. (30) encountered in the context of the one-site breather.
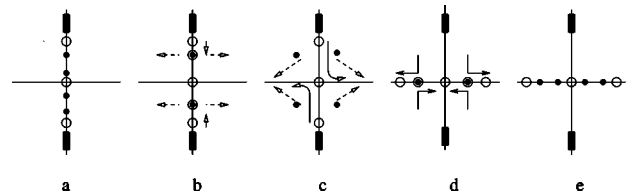

FIG. 12. Sequence of changes in the disposition of growth rates in the complex plane; thick black lines denote the band while the dots and circles correspond to localized modes: (a) before Krein collision ($\gamma<\gamma_K^s$; λ fixed); (b) Krein collision $\gamma=\gamma_K^s$; (c) a quartet of complex growth rates resulting from the Krein collision, and a pair of imaginary growth rates approaching collision at $p=0$; (d) Krein collision in reverse; (e) all growth rates of localized modes real.
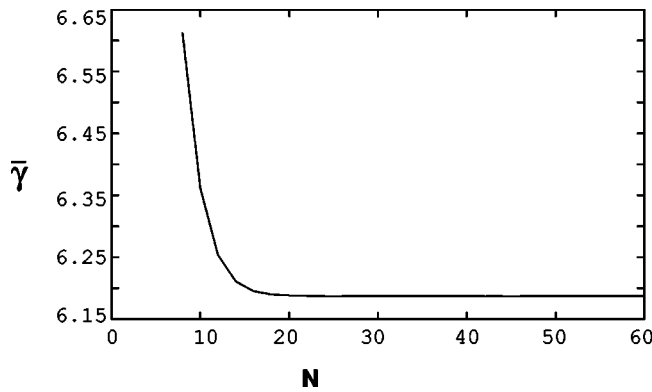
FIG. 13. Variation of $\bar{\gamma}$ with N for fixed λ ($=0.5$).

(viii) Thus, it is of interest to look at the sequence of events for *large N* as one varies γ for any given λ. As one expects, the breather profile around each of the high sites approaches the one-site profile given by Eq. (6) [recall the arbitrariness of the overall phase factor in Eq. (6)] for $N \rightarrow \infty$. In this situation, each of the symmetric modes is associated with a corresponding antisymmetric mode (one of which is the trivial mode at $\mu=0$) forming a nearly degenarate pair. One thus has two pairs of nearly degenerate eigenvalues—one near $\mu=0$ and the other appearing at the inner band edge at $\gamma \approx \gamma_1(\lambda)$ [one notes from Fig. 10 that for large N $\gamma_{th}^{(s)} \approx \gamma_{th}^{(a)} \approx \gamma_1(\lambda)$]. As γ is made to increase beyond $\gamma_1(\lambda)$, this latter pair moves toward $\mu=0$, until at $\gamma \approx \bar{\gamma}(\lambda)$ a Krein collision takes place, followed closely by a double-zero configuration. In other words, the sequence of dispositions depicted in Fig. 12 all occur closely on the heels of one another close to $\mu=0$, $\gamma=\bar{\gamma}(\lambda)$.

V. CONCLUDING REMARKS

In summary, we have supplemented our earlier work on the discrete nonlinear Schrödinger type model (1),(2) by constructing an exact two-site antiphase breather solution (39a)–39c) [a more general solution with phase difference δ between the high sites is given by Eqs. (36a)–(36c)], and by presenting a complete stability analysis for both the one-site and two-site breathers. While the one-site breather gets destabilized by the temporal growth of a zero-frequency mode, the two-site breather is destabilized through the growth of an oscillating mode. Hence one can predict the types of structures that appear beyond the instability in these two cases: while the one-site breather breaks up to yield a multisite breather of the same frequency, the two-site breather yields a multifrequency breather beyond the instability. The model also yields a host of other exact single-frequency breather solutions such as the two-site breathers with an arbitrary phase difference δ alluded to above. The value of δ is crucial for the stability of the breather: while antiphase breathers are stable for parameter values λ, γ lying in some region of the parameter space, in-phase breathers are seen to be always unstable. Other exact solutions yielded by the model are multisite breathers with, say, a number m of high sites ($m > 2$) characterized by a sequence of gaps $N_1, N_2, \ldots, N_{m-1}$ and phase differences $\delta_1, \delta_2, \ldots, \delta_{m-1}$. It would be interesting to look into the stability characteristics of these exact vortex-type breather solutions and to see if stable breathers of this type with *chaotic* sequences of gap lengths and phase differences are allowed in the model.

---

[1] S. Flach and C.R. Willis, Phys. Rep. **295**, 181 (1998).

[2] M. Johansson and S. Aubry, Phys. Rev. E **61**, 5864 (2000).

[3] P.G. Kevrekidis, K.Ø. Rasmussen, and A.R. Bishop, Phys. Rev. E **61**, 4652 (2000).

[4] M. Kollmann, H.W. Capel, and T. Bountis, Phys. Rev. E **60**, 1195 (1999).

[5] V.V. Konotop and S. Takeno, Phys. Rev. E **60**, 1001 (1999).

[6] R.E. Amritkar and V.M. Kenkre, Phys. Rev. E **59**, 6306 (1999).

[7] D. Hennig, Phys. Rev. E **59**, 1637 (1999).

[8] J.M. Hyman, D.W. Mclaughlin, and A.C. Scott, Physica D **3**, 23 (1981).

[9] G. Careri, U. Buontempo, F. Carta, E. Gratton, and A.C. Scott, Phys. Rev. Lett. **51**, 304 (1983).

[10] J.C. Eilbeck, P.S. Lomdahl, and A.C. Scott, Physica D **16**, 318 (1985).

[11] T. Holstein, Ann. Phys. (N.Y.) **8**, 325 (1959).

[12] *Future Directions of Nonlinear Dynamics in Physical and Biological Systems*, edited by P.L. Christiansen, J.C. Eilbeck, and R.D. Parmentier, special issue of Physica D **68**, 116 (1993).

[13] R.S. McKay and S. Aubry, Nonlinearity **7**, 1623 (1994).

[14] A. Lahiri, S. Panda, and T.K. Roy, Phys. Rev. Lett. **84**, 3570 (2000).

[15] P.J. Martinez, L.M. Floria, J.L. Marin, S. Aubry, and J.J. Mazo, Physica D **119**, 175 (1998).

[16] P. Binder, D. Abraimov, A.V. Ustinov, S. Flach, and Y. Zolotaryuk, Phys. Rev. Lett. **84**, 745 (2000).

[17] P.G. Kevrekidis, K.Ø. Rasmussen, and A.R. Bishop, Phys. Rev. E **61**, 2006 (2000).

[18] E.W. Laedke, O. Kluth, and K.H. Spatschek, Phys. Rev. E **54**, 4299 (1996).

[19] M. Johansson, S. Aubry, Y.B. Gaididei, P.L. Christiansen, and K.Ø. Rasmussen, Physica D **119**, 115 (1998).

[20] P.G. Kevrekidis, K.Ø. Rasmussen, and A.R. Bishop, Int. J. Mod. Phys. B **15**, 2833 (2001).

[21] S. Aubry, Physica D **103**, 201 (1997).

[22] R.S. MacKay and J.A. Sepulchre, Physica D **119**, 148 (1998).

[23] A. Lahiri and M. Sinha Roy, Int. Jour. Nonlin. Mech. **36**, 787 (2001).

[24] T.J. Bridges and J.E. Furter, *Singularity Theory and Equivariant Symplectic Maps* (Springer-Verlag, Berlin, 1993).

[25] M.B. Sevryuk and A. Lahiri, Phys. Lett. A **154**, 104 (1991).